2014 International Joint Conference on Neural Networks (IJCNN)
July 6-11, 2014, Beijing, China

Nonlinear responses of an asynchronous cellular automaton model of spiral ganglion cell

Masato Izawa and Hiroyuki Torikai, *Member, IEEE*

***Abstract*— The mammalian cochlear consists of nonlinear components: lymph (viscous fluid), a basilar membrane (vibrating membrane), outer hair cells (active dumpers), inner hair cells (neural transducers), and spiral ganglion cells (parallel spikes density modulators). In this paper, a novel spiral ganglion cell model based on an asynchronous sequential logic is presented. It is shown that the presented model can reproduce typical nonlinear responses of the spiral ganglion cell, e.g., spontaneous spiking, parallel spike density modulation, and adaptation. Also, FPGA experiments validate the reproductions of the nonlinear responses by the presented model.**

I. Introduction

THE mammalian ear is divided into an outer ear, a middle ear, and an inner ear, where a sound processing is mainly executed in a cochlear of the inner ear. Fig. 1 shows a sketch of a mammalian cochlear [1], which consists of a stapes, lymph, a basilar membrane, outer hair cells (not shown in the figure), inner hair cells, and spiral ganglion cells. In the cochlear, a sound stimulation via the stapes induces vibrations of the lymph and the basilar membrane, which work together to realize a mechanical Fourier transformation in such a way that higher and lower frequency components in the sound stimulation induce vibrations near and far from the stapes, respectively. As shown in Fig. 1, many inner hair cells are attached to the basilar membrane, where their locations correspond to frequency components in the Fourier transformed sound stimulation. Each inner hair cell transforms the mechanical vibration with its own frequency (called the characteristics frequency [1]) into its internal electrical potential $s_{rec}(t)$ called a receptor potential. As shown in Fig. 1, N spiral ganglion cells are attached to one inner hair cell, where their number N is about 20 in the case of the human. The N spiral ganglion cells encode the receptor potential $s_{rec}(t)$ of the inner hair cell into parallel spike-trains $\{Y_1(t), \cdots, Y_N(t)\}$, which are transmitted to the central nervous system. Due to its high nonlinearities, the cochlear exhibits a huge variety of nonlinear responses such as nonlinear band-pass filtering, missing fundamental, multi-tone suppression, first and second pitch shifts, otoacoustic emission, rectifying, density modulation of the sound stimulation, parallel spike modulation, adaptation of spike density, and so on [1]-[9]. In order to understand such complicated nonlinear responses, many mathematical models have been presented and analyzed intensively [9]-[24]. In addition to such fundamental researches (i.e., biological measurements and mathematical modelings), many artificial electronic cochleas have been presented for engineering as well as clinical applications [18]-[22]. In such applications, hardware cost is always a big issue. Recently, several types of asynchronous sequential logic neuron models have been presented the advantages of which include low hardware cost and on-chip learning capability [24]-[27]. So, in this paper, based on the asynchronous sequential logic neuron model, a novel spiral ganglion cell model is presented. First, in section II, the novel spiral ganglion cell model is presented and its asynchronous dynamics is explained. Second, in section III, design procedures of the presented model are presented. Also, in order to support these design procedures, some conjectures are provided, where their proofs are omitted due to the page number limitation and will be presented in a future journal paper. It is shown that the designed model can reproduce typical nonlinear responses of the spiral ganglion cell, e.g., spontaneous spiking, parallel spike density modulation, and adaptation. Third, in section IV, FPGA experiments validate the reproductions of the nonlinear responses by the presented model.

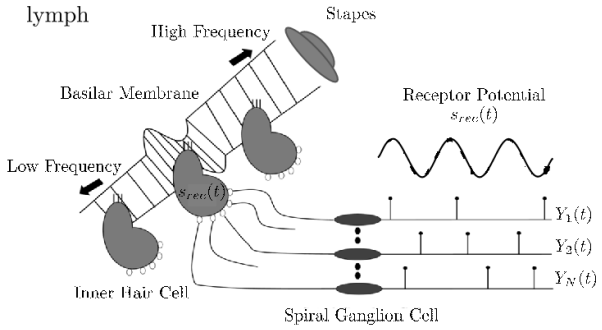

Fig. 1. A sketch of the mammalian cochlea [1].

Novelties and significances of this paper are many, including the following points.

- Most asynchronous sequential logic neuron models are designed to reproduce the nonlinear dynamics of neurons in the central nervous system [25]-[27]. On the other hand, this paper presents the asynchronous sequential logic model of the cell in the cochlea *for the first time*.
- Most traditional cochlea models (i.e., models of both

M. Izawa is with the Department of Systems Innovation, Graduate School of Engineering of Science, Osaka University, Toyonaka, Japan (e-mail: izawa@hopf.sys.es.osaka-u.ac.jp).

H. Torikai is with the Department of Computer Science, Faculty of Computer Science and Engineering, Kyoto Sangyo University(e-mail: torikai@cse.kyoto-su.ac.jp).

This work was partially supported by the support center for advanced telecommunications technology research (SCAT) and KAKENHI Grant Number 24700225

978-1-4799-1484-5/14/$31.00 ©2014 IEEE

cochlea components and whole cochlea) are described by ordinary and/or partial differential equations, which have continuous states and a continuous time. On the other hand, the asynchronous sequential logic spiral ganglion cell model has discrete states and a continuous (state transition) time. *Hence the dynamics of the presented model is described by an asynchronous cellular automaton, which belongs to a different class of dynamical system from the traditional cochlea models.* It should be emphasized that, from a standpoint of fundamental research, such a new modeling approach of a biological system *per se* is an important research theme.

• The presented spiral ganglion cell model will be a bridgehead to design a whole cochlea model based on the asynchronous sequential logic. Recall that the asynchronous sequential logic neuron models have the advantages of the low hardware cost and the on-chip learning capability. Hence a future asynchronous sequential logic cochlea model will also have the same advantages both of which are beneficial for applications, e.g., a low hardware cost cochlea implant with after implant parameter optimization capability.

II. Asynchronous sequential logic model of paralleled spiral ganglion cells

A. Spike-density-based inner hair cell model

As explained in Fig. 1, N spiral ganglion cells are parallelly connected to one inner hair cell in the mammalian inner ear, where N is about 20 in the case of the human. Before presenting a novel spiral ganglion cell model in the next subsection, the inner hair cell model in Fig.2(a) (which is based on our previous neuron models and is out of detailed consideration in this paper) is briefly explained in this subsection. The signal $s_{rec}(t)$ corresponds to a receptor potential of the inner hair cell, where $t \in [0, \infty)$ is a continuous time. The receptor potential $s_{rec}(t)$ can be assumed to be a sinusoidal wave since the basilar membrane works as a Fourier transformer. Then, the following receptor potential $s_{rec}(t)$ is focused on in this paper.

$$s_{rec}(t) = a(\sin(2\pi f t) + 1),$$

where $f > 0$ is an input frequency and $a \geq 0$ is a parameter. Our group is developing neuron models in which potentials are represented by spike densities. In this paper, such a spike-density-based neuron model is assumed to be used as the inner hair cell model and thus the receptor potential $s_{rec}(t)$ is assumed to be represented by a spike density as follows.

$$s(t) = \begin{cases} 1 & \text{if } t = t_1, t_2, \cdots, \\ 0 & \text{otherwise,} \end{cases} \tag{1}$$

where $\{t_1, t_2, \cdots\}$, $t_n \in [0, \infty)$, are spike positions and the shape of the density of the spike positions $\{t_1, t_2, \cdots\}$ is assumed to be proportional to the waveform of the receptor potential $s_{rec}(t)$. The spike-train $s(t)$ is used as a stimulation spike-train to the spiral ganglion cell model presented in the next subsection.

B. Novel paralleled spiral ganglion cell models

In this subsection, a novel asynchronous sequential logic model (i.e., electronic circuit model) of the spiral ganglion cell is presented. Fig. 2(a) shows a sketch of the paralleled structure of the models. The spike-train $s(t)$ is a *stimulation spike-train* to the N paralleled *ganglion cell units* (ab. GCUs), where the GCU corresponds to the spiral ganglion cell. Each i-th GCU has a discrete state $X_i(t)$, which corresponds to a membrane potential of the spiral ganglion cell and thus is called a *membrane potential*. The *reset value unit* (ab. RVU) generates a discrete *reset value* $R(t)$ to which the membrane potential $X_i(t)$ is reset when the i-th GCU fires. The role of the reset value $R(t)$ is explained later in Remark 2. As shown in Fig. 2(a), The GCUs and the RVU accept the following *threshold modulation clock* $C_\Theta(t)$.

$$C_\Theta(t) = \begin{cases} 1 & \text{if } t = 0, dT_i, 2dT_i, \cdots, \\ 0 & \text{otherwise,} \end{cases} \tag{2}$$

where $d > 0$ and $T_i > 0$ are real parameters.

Dynamics of RVU: In Figs. 2(b), a diagram of the RVU is shown. The RVU has the M-bit register, which is used in the one-hot coding manner, i.e., only one bit is 1 and the other bits are 0s for all t. Then the register has the following discrete state.

$$P(t) \in \boldsymbol{Z}_M = \{0, 1, ..., M-1\}, \quad M \geq 2.$$

As explained in the table in Fig. 2, the discrete state $P(t)$ determines the shape of the reset value $R(t)$. The RVU also has the J-bit one-hot-coded register, which has the following discrete state.

$$Q(t) \in \boldsymbol{Z}_J = \{0, 1, ..., J-1\}, \quad J \geq 2.$$

As explained in the table in Fig. 2, the discrete state $Q(t)$ modulates the shape of the following *threshold signal* $T(t)$.

$$T(t) = \begin{cases} \mu Q(t) + \lambda - 1 & \text{if } \mu Q(t) + \lambda - 1 < M - 1, \\ M - 1 & \text{if } \mu Q(t) + \lambda - 1 \geq M - 1. \end{cases} \tag{3}$$

As explained in the table in Fig. 2, the threshold signal $T(t)$ is introduced to realize an adaptation. As shown in Fig. 2(b), the RVU accepts the following *internal clock.*

$$C_R(t) = \begin{cases} 1 & \text{if } t = T_i, 2T_i, \cdots, \\ 0 & \text{otherwise,} \end{cases}$$

where T_i is a period. Then, the state transitions in the RVU are described by the following equation.

$$P(t_+) := \begin{cases} P(t)+1 & \text{if} \quad s(t) = 1 & \text{and } P(t) < T(t), \\ 0 & \text{if} \quad s(t) = 1 & \text{and } P(t) \geq T(t), \\ P(t)+1 & \text{if} \quad C_R(t) = 1 & \text{and } P(t) < T(t), \\ 0 & \text{if} \quad C_R(t) = 1 & \text{and } P(t) \geq T(t), \end{cases}$$

$$Q(t_+) := \begin{cases} Q(t)-1 & \text{if} \quad C_\Theta(t) = 1 & \text{and } Q(t) > 0, \\ Q(t)+1 & \text{if} \quad P(t) = 0 & \text{and } Q(t) < J-1, \end{cases} \tag{4}$$

where the symbol "t_+" denotes $\lim_{\epsilon \to +0} t + \epsilon$ and the symbol ":=" denotes an instantaneous state transition hereafter. The

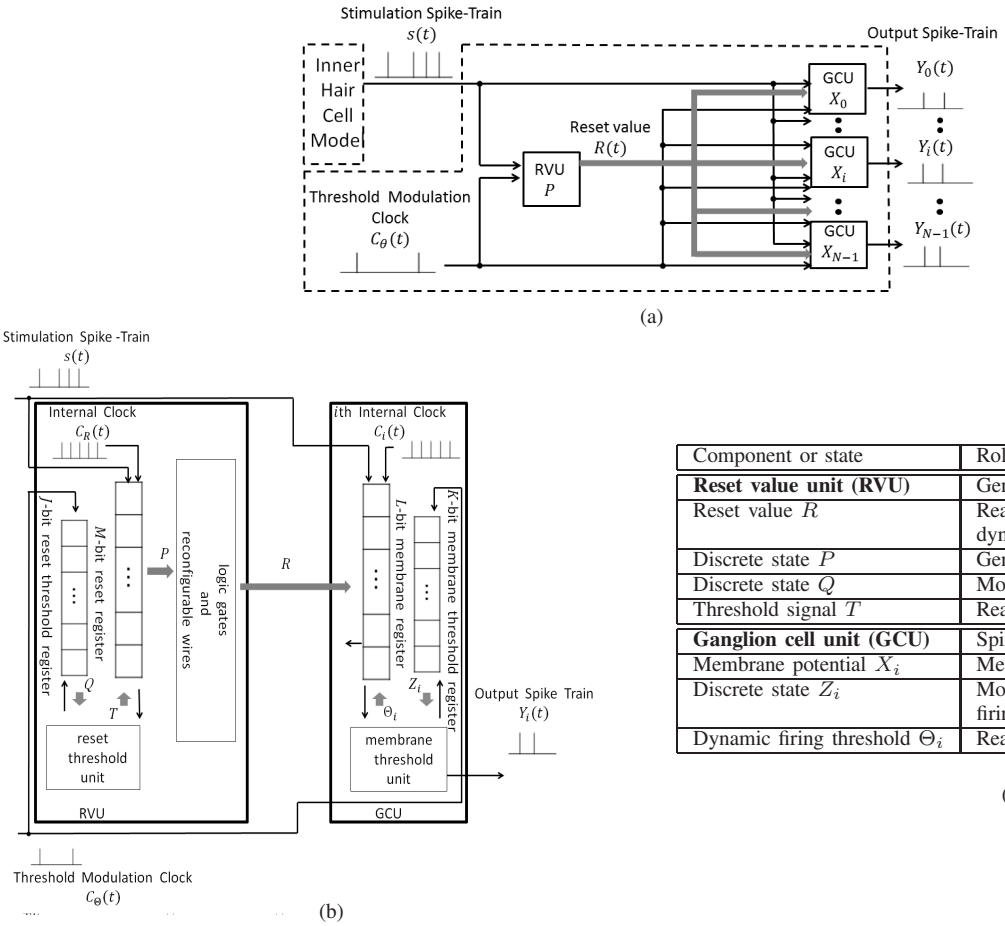

Component or state	Role or meaning
Reset value unit (RVU)	Generation of reset value R
Reset value R	Realization of nonlinear dynamics of GCU
Discrete state P	Generation of reset value R
Discrete state Q	Modulation of threshold signal T
Threshold signal T	Realization of adaptation
Ganglion cell unit (GCU)	Spiral ganglion cell model
Membrane potential X_i	Membrane potential
Discrete state Z_i	Modulation of Dynamic firing threshold Θ_i
Dynamic firing threshold Θ_i	Realization of adaptation

(c)

Fig. 2. Schematic drawing of the spiral ganglion cell model. (a) Whole system consists of paralleled N asynchronous sequential logic model of spiral ganglion cells. (b) Reset value unit and ganglion cell unit. (c) Role or meaning of component or state.

discrete states $P(t)$ and $Q(t)$ are clamped to the ranges $\boldsymbol{Z}_M$ and $\boldsymbol{Z}_J$, respectively. In Fig. 3, typical waveforms of the discrete state $P(t)$ and the threshold signal $T(t)$ are shown. The discrete state $P(t)$ basically increases. But if the discrete state $P(t)$ reaches the threshold signal $T(t)$ and a clock $C_R(t) = 1$ or an stimulation spike $s(t) = 1$ arrives, then the discrete state $P(t)$ is reset to 0 as indicated by the arrow 1 in Fig. 3. After the reset, the discrete state $P(t)$ again increases. Using the discrete states (P, Q), the RVU generates the following *reset value* $R(t)$.

$$R(t) = T(t) - P(t) \in \{0, 1, ..., M-1\}.$$

Dynamics of GCU: In Figs. 2(b), a diagram of the i-th GCU is shown. The GCU has the L-bit one-hot-coded *membrane register*, which has the following discrete *membrane potential.*

$$X_i(t) \in \boldsymbol{Z}_L = \{0, 1, ..., L-1\}, \quad L \geq 2.$$

As explained in the table in Fig. 2, the membrane potential $X_i(t)$ corresponds to the membrane potential of the mammalian spiral ganglion cell. The GCU also has the K-bit one-hot-coded *adaptation register*, which has the following discrete state.

$$Z_i(t) \in \boldsymbol{Z}_K = \{0, 1, ..., K-1\}, \quad K \geq 2.$$

As explained in the table in Fig. 2, the discrete state $Z_i(t)$ modulates the shape of the following *dynamic firing threshold* $\Theta_i(t)$.

$$\Theta_i(t) = \begin{cases} \alpha Z_i(t) + \beta - 1, & \text{if } \alpha Z_i(t) + \beta - 1 < L - 1, \\ L - 1, & \text{if } \alpha Z_i(t) + \beta - 1 \geq L - 1. \end{cases} \tag{5}$$

As explained in the table in Fig. 2, the dynamic firing threshold $\Theta_i(t)$ is introduced to realize the adaptation. As shown in Fig. 2(b), the i-th GCU accepts the following *internal clock*.

$$C_i(t) = \begin{cases} 1 & \text{if } t = T_i + T_i\phi_i, 2T_i + T_i\phi_i, \cdots, \\ 0 & \text{otherwise} \end{cases}$$

where $0 \leq \phi_i < 1$, $\phi_i \neq \phi_j$, $i \neq j$. Then, the state transitions in the GCU are described by the following

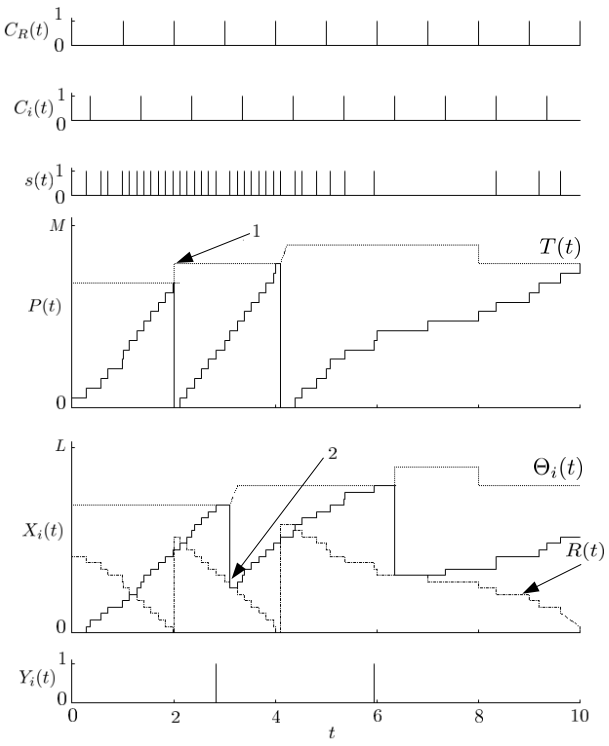

Fig. 3. Basic dynamics of the RVU and the GCU.

equation.

$$X_i(t_+) := \begin{cases} X_i(t)+1 & \text{if } s(t)=1 \quad \text{and } X_i(t) < \Theta_i(t), \\ R(t) & \text{if } s(t)=1 \quad \text{and } X_i(t) \geq \Theta_i(t), \\ X_i(t)+1 & \text{if } C_i(t)=1 \quad \text{and } X_i(t) < \Theta_i(t), \\ R(t) & \text{if } C_i(t)=1 \quad \text{and } X_i(t) \geq \Theta_i(t), \end{cases}$$

$$Z_i(t_+) := \begin{cases} Z_i(t)-1 & \text{if } C_\Theta(t)=1 \quad \text{and } \Theta_i(t) > 0, \\ Z_i(t)+1 & \text{if } X_i(t)=R(t) \quad \text{and } \Theta_i(t) < K-1, \end{cases} \tag{6}$$

where the membrane potential $X_i(t)$ and the discrete state $Z_i(t)$ are clamped to the ranges $\boldsymbol{Z}_L$ and $\boldsymbol{Z}_K$, respectively. In Fig. 3, typical waveforms of the membrane potential $X_i(t)$, the dynamic firing threshold $\Theta_i(t)$, and the reset value $R(t)$ are shown. As show in this figure, the membrane potential $X_i(t)$ basically increases. But if the membrane potential $X_i(t)$ reaches the dynamic firing threshold $\Theta_i(t)$ and an internal clock $C_i(t) = 1$ or an stimulation spike $s(t) = 1$ arrives, then the membrane potential $X_i(t)$ is reset to the reset value $R(t)$ as indicated by the arrow 2 in Fig. 3. Repeating the resets, the i-th GCU generates the following *output spike-train* $Y_i(t)$.

$$Y_i(t) = \begin{cases} 1 & \text{if } s(t)=1 \text{ and } X_i(t) \geq \Theta_i(t), \\ 0 & \text{otherwise.} \end{cases} \tag{7}$$

As a result, the presented GCUs and RVU are described by Equations (3), (4), (5), (6), and (7), and are characterized by the following parameters.

$$N,\ M,\ L,\ J,\ K,\ \alpha,\ \mu,\ \beta,\ \lambda,\ d,\ T_i,\ \phi_i.$$

C. Problem statement

The spiral ganglion cells in the mammalian inner ear exhibit a variety of nonlinear phenomena. Among them, the following major ones are focused on in this paper.

Spontaneous spiking: The spiral ganglion cell generates a spike-train $y_i(t)$ without sound stimulation as shown in Fig. 4(a) [3]. Such a phenomenon is called a *spontaneous spiking*.

Parallel spike density modulation: N spiral ganglion cells are parallelly connected to one inner hair cell and the receptor potential $s_{rec}(t)$ of the inner hair cell is modulated into the paralleled N spike-trains $\{Y_1(t), \cdots, Y_N(t)\}$. A spike density of the sum of the N spike-trains mimics the waveform of the receptor potential $s_{rec}(t)$ as shown in Figs. 4(b) and (b') [3]. In this paper, such an modulation is referred to as a *parallel spike density modulation*.

Adaptation: The spiral ganglion cell generates higher density spikes at an onset of a sound stimulation as shown in Fig. 4(c) [2]. Such a phenomenon is called an *adaptation*.

In the following sections, the following problems are studied.

(Sec. III.A) Design of the GCU and the RVU to reproduce a given spontaneous spike density as well as theoretical analysis of the designed model.

(Sec. III.B) Design of the GCUs and the RVU to reproduce the parallel spike density modulation as well as theoretical and numerical analyses of the designed model.

(Sec. III.C) Design of the GCUs and the RVU to reproduce the adaptation as well as detailed numerical analysis of the designed model.

The presented GCUs and RVU have the following features.

Remark 1 (features of the presented model):
(1) The presented model (i.e., the GCUs and the RVU) has the discrete states (P, Q, X_i, Z_i) and their transitions can occur asynchronously. Hence, from a viewpoint of nonlinear dynamical system theory, the presented model can be regarded as an *asynchronous cellular automaton*, which is especially designed to reproduce nonlinear responses of the mammalian spiral ganglion cell.
(2) Our group has developed several types of neuron models based on the asynchronous cellular automaton [24]-[27]. This paper present the asynchronous cellular automaton model of the spiral ganglion cell for the first time.
(3) From a viewpoint of circuit implementation, the presented model can be regarded as an asynchronous sequential logic and thus it is suitable for FPGA implementation.

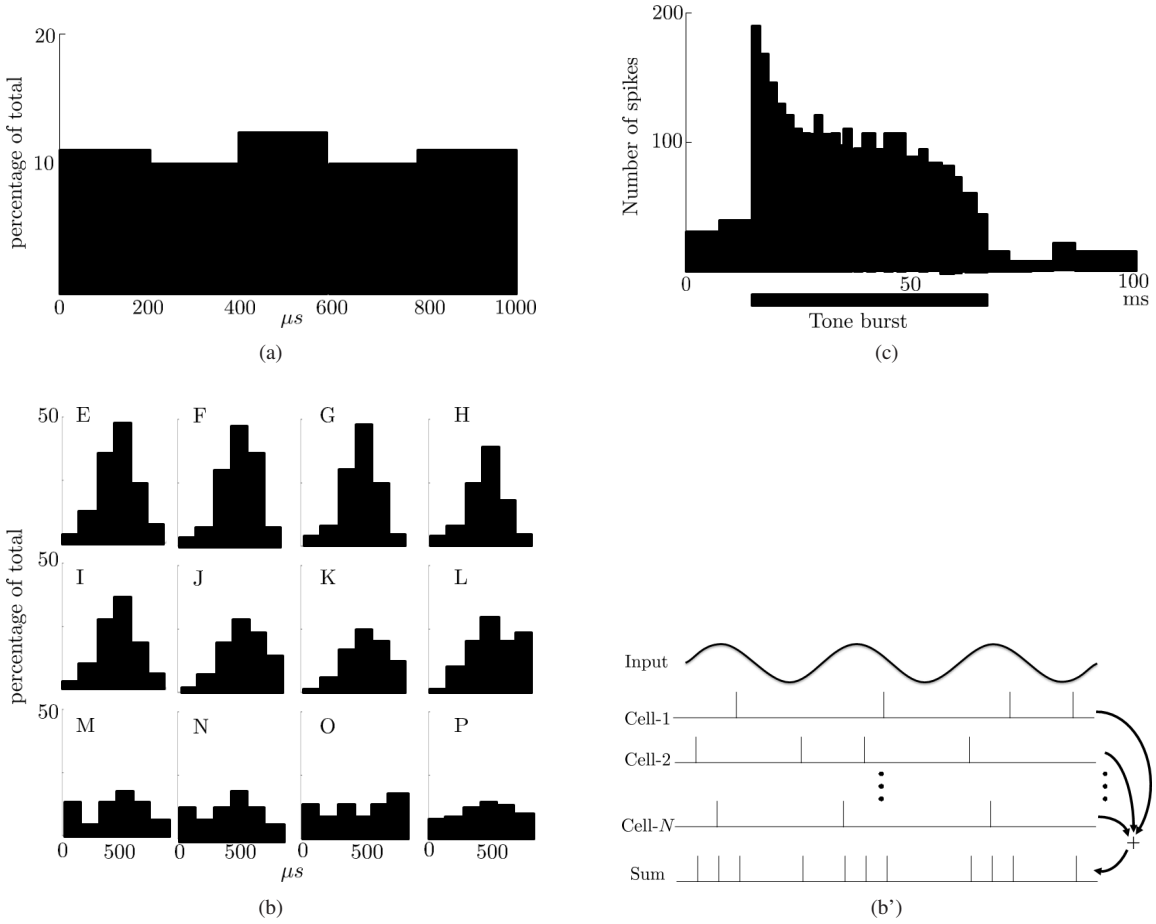

Fig. 4. Measured data from squirrel monkey ((a) and (b)) [3] and cat ((c) and (b')) [1]. (a) Spontaneous firing. (b) Spike density modulation of parallel spike density modulation. (b') Parallel spike modulation of parallel spike density modulation. (c) Adaptation.

III. Design and analysis

A. Design and analysis to reproduce spontaneous spiking

Let us begin with introducing the following spike density $\gamma(y)$ of a spike-train $y(t)$.

$$\gamma(y) = \lim_{\tau\to\infty} \frac{\text{The number of spikes } y(t) = 1 \text{ for } t \in [0, \tau]}{\tau}. \tag{8}$$

Instead of the ideal case $\tau \to \infty$, a realistic case $\tau = 1000$ is used for numerical simulations in this paper.

Recall that Fig. 4(a) shows the measured spontaneous spiking of the spiral ganglion cell. Now we treat such a measured spontaneous spike density as a given one and want to reproduce it by the presented model. Let such a measured spontaneous spike density be denoted by γ_{given}. We then propose the following design procedure of the GCU and the RVU so that they reproduce the given spontaneous spike density γ_{given}.

Design procedure A: The length M of the register is set to an even number, where M determines the resolutions of the discrete states (P, Q, X_i, Z_i). The period of the clocks is set to $T_i = 1/(M\gamma_{given})$. The other parameters are set to $L = \frac{3}{2}M$, $J = 0$, $K = 0$, $\alpha = 0$, $\mu = 0$, $\beta = L$, and $\lambda = M$. Note that since this design procedure is for a single GCU, the number N is not treated as a parameter here.

Figs. 5(a) and (b) show numerical simulation results under the above design. It can be confirmed that the resulting spontaneous spike densities $\gamma(Y_i)$ match with the given ones. Concerning the design procedure A, the following conjecture is given.

Conjecture A: Assume the GCU and the RVU satisfy the following parameter condition.

$$L = \frac{3}{2}M,\ J = 0,\ K = 0,\ \alpha = 0,\ \mu = 0,\ \beta = L,\ \lambda = M. \tag{9}$$

Then, the spike density $\gamma(Y_i)$ of the spike-train $Y_i(t)$ of the GCU is given by

$$\gamma(Y_i) = (1 + \gamma(s))/(MT_i),$$

where $\gamma(s)$ is the density of the stimulation spike-train $s(t)$.

Proof of the Conjecture A is omitted due to the page number limitation. Based on the Conjecture A, we have the following corollary.

Corollary A: The Conjecture A guarantees that the design

Fig. 5. Examples of the Conjecture A. (a) Spontaneous spiking. The parameters are $(N, M, L, J, K, \alpha, \mu, \beta, \lambda) = (1, 118, 177, 0, 0, 0, 0, 177, 118)$. The spike density $\gamma(Y_i) \simeq 7.62 \times 10^{-3}$ by a numerical simulation matches with a given spike density $\gamma_{given} = 8.47 \times 10^{-3}$. (b) Stimulation-induced firing. The parameters are $(N, M, L, J, K, \alpha, \mu, \beta, \lambda) = (1, 118, 177, 0, 0, 0, 0, 177, 118)$. The spike density $\gamma(Y_i) \simeq 1.08 \times 10^{-1}$ by a numerical simulation matches with a given spike density $\gamma_{given} = 1.09 \times 10^{-1}$.

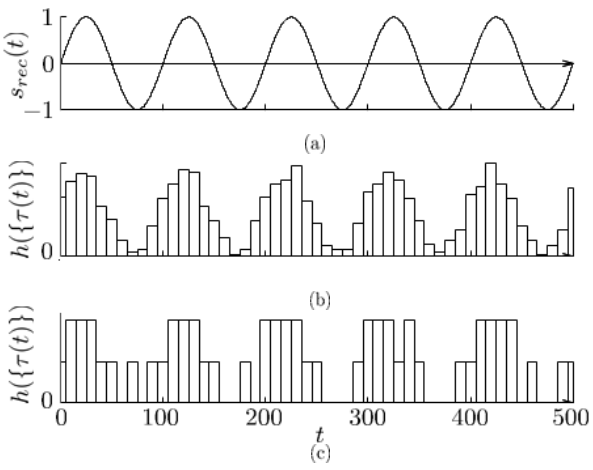

Fig. 6. Parallel spike density modulations. (a) Receptor potential $s_{rec}(t)$. (b) Histogram h of the logical sum of the 20 output spike-trains $\{Y_1(t), \cdots, Y_N(t)\}$ from the presented model. The parameters are $(N, M, L, J, K, \alpha, \mu, \beta, \lambda, d, T_i, \phi_i) = (20, 118, 177, 0, 0, 3, 2, 177, 118, 0\ 1\ \sqrt{3}i/35)$. The initial states are set to the same value $X_i(0) = X_j(0) = 0$. (c) Histogram h of the logical sum of the 20 output spike-trains $\{Y_1(t), \cdots, Y_N(t)\}$ from the presented model *without* the RVU. The parameters are $(N, M, L, J, K, \alpha, \mu, \beta, \lambda, d, T_i, \phi_i) = (20, 0, 118, 0, 0, 3, 0, 118, 0, 0\ 1\ \sqrt{3}i/35)$. The initial states are set to the same value $X_i(0) = X_j(0) = 0$.

procedure A leads to the reproduction of the given spontaneous spike density $\gamma(Y_i) = \gamma_{given}$ by the GCU and the RVU.

B. Design and analysis to reproduce parallel spike density modulation

Recall that Figs. 4(b) and (b') show the measured parallel spike density modulation. In this subsection, we propose the following design procedure of the GCUs and the RVU so that they reproduce the parallel spike density modulation.

Design procedure B: The length M of the register is set to an even number, where M determines the resolutions of the discrete states (P, Q, X_i, Z_i). The other parameters are set to $L = \frac{3}{2}M$, $J = 0$, $K = 0$, $\alpha = 0$, $\mu = 0$, $\beta = L$, $\lambda = M$, and $T_i = 1/(M\gamma_{given})$. The number N of the GCUs is set to 20 same as the human. The initial phases of the internal clocks are set to $\phi_i \neq \phi_j$, $i \neq j$.

In order to analyze the parallel spike density modulation, let us introduce the following histogram $h(\{\tau(n)\})$ of spike positions $\{\tau(1), \tau(2), \cdots, \tau(n), \cdots\}$.

$$h(\{\tau(n)\}) = \text{Histogram of the spike positions } \{\tau(n)\} \text{ for a bin width } \epsilon.$$

Fig. 6(b) show a histogram $h(\{\tau(n)\})$ of the spike positions $\{\tau(1), \tau(2), \cdots, \tau(n), \cdots\}$ of the sum $Y(t)$ of the spike-trains $\{Y_1(t), \cdots, Y_N(t)\}$ under the design procedure B. It can be confirmed that the histogram $h(\{\tau(n)\})$ in Fig. 6(b) mimics the receptor potential $s_{rec}(t)$ in Fig. 6(a), i.e., the resulting GCUs and the RVU can realize the parallel spike density modulation.

Remark 2 (Role of the RVU): In Fig. 6(c), the reset value $R(t)$ is fixed to a constant value, i.e., the RVU is removed. It can be seen that, in this case, the histogram $h(\{\tau(1), \tau(2), \cdots\})$ of the spike positions $\{\tau(1), \tau(2), \cdots\}$ of the sum $Y(t)$ of the spike-trains $\{Y_1(t), \cdots, Y_N(t)\}$ does not mimic the shape of the receptor potential $s_{rec}(t)$. This is the reason why the RVU is needed to reproduce the parallel spike density modulation. Explanations of the mechanism of this reason is too long for this conference paper and will be presented in a future journal paper.

Remark 3 (Design procedures A and B): Note that the design procedure B satisfies Proposition A, i.e., under the design procedure B, the GCUs and the RVU reproduce not only the parallel spike density modulation (as explained in this subsection) but also a given spike density (as explained in the previous subsection).

C. Design and analysis to reproduce adaptation

Recall that Fig. 4(c) shows the measured adaptation of the spiral ganglion cell. In this subsection, we propose the following design procedure of the GCU and the RVU so that they reproduce the adaptation.

Design procedure C: The length M of the register is set to an even number, where M determines the resolutions of the discrete states (P, Q, X_i, Z_i). The other parameters are set to $M = 182, L = \frac{3}{2}M$, $J = 64$, $K = 64$, $\alpha = 3$, $\mu = 2$, $\beta = L - \alpha J$, $\lambda = M - \beta K$, and $T_i = 1/(M\gamma_{given})$. The number N of the GCUs is set to 20 same as the human.

Fig. 7(a) shows a histogram $h(\{\tau(1), \tau(2), \cdots\})$ of the spike positions $\{\tau(1), \tau(2), \cdots\}$ of the sum $Y(t)$ of the N spike-trains $\{Y_1(t), \cdots, Y_N(t)\}$ under the design procedure C. It can be confirmed in this figure that the GCUs and the RVU reproduce the adaptation, i.e., the histogram h is higher at the onset of the stimulation spike-train $s(t)$ and then gradually decreases. Fig. 7(b) and (c) explain a mechanism of the realization of the adaptation. Fig. 7(b) is a magnified

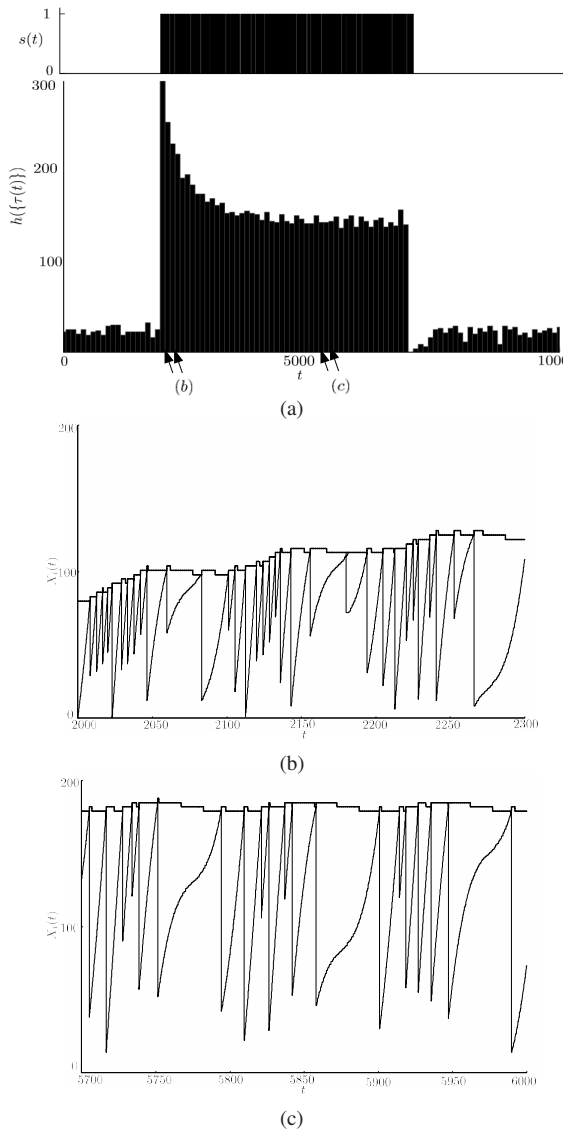

Fig. 7. Adaptation. (a) Stimulation spike-train $s(t)$ and histogram $h(\{\tau(1), \tau(2), \cdots\})$ of the spike positions $\{\tau(1), \tau(2), \cdots\}$ of the sum $Y(t)$ of the N spike-trains $\{Y_1(t), \cdots, Y_N(t)\}$ under the design procedure C. The parameters are $(N,\ M,\ L,\ J,\ K,\ \alpha,\ \mu,\ \beta,\ \lambda,\ d,\ T_i,\ \phi_i) = (20,\ 182,\ 273,\ 64,\ 64,\ 3,\ 2,\ 81,\ 54,\ 52,\ 1,\ \sqrt{3}i/35)$. (b) and (c) are magnifications of (a).

waveforms around the onset of the stimulation spike-train $s(t)$ (see the two arrows in Fig. 7(a) at $t = 2000$ and $t = 2300$). It can be seen that the dynamics firing threshold $\Theta_i(t)$ changes and adjusts the firing rate. Fig. 7(c) is a magnified waveforms around a steady state (see the two arrows in Fig. 7(a) at $t = 5700$ and $t = 6000$). It can be seen that the dynamics firing threshold $\Theta_i(t)$ does not change so much and the firing rate is almost constant.

IV. FPGA IMPLEMENTATION

The RVU and the 20 GCUs are implemented in a *field programmable gate array* (ab. FPGA). The dynamics of the GCUs and the RVU are described by Equations (3), (4), (5), (6), and (7), which are written in a VHDL source code. A bitstream file for the FPGA configuration is generated by Xilinx's design software environment ISE 14.4. Table 1 shows parameters of the GCUs and the RVU and specifications of the resulting FPGA, where binary coding is automatically used to represent the discrete states (P, Q, X_i, Z_i) by the ISE. The clocks $C_R(t)$, $C_i(t)$, and $C_\theta(t)$ are generated by an on-board 100[MHz] clock and a frequency divider. Since the FPGA and the design software we used do not support for asynchronous triggering, the stimulation spike-train $s(t)$ is sampled at the on-board clock frequency. Note that the sampling of $s(t)$ is not necessary if a target FPGA supports for asynchronous triggering. Fig. 8 shows typical time waveforms from the GCUs and the RVU. It can be seen in this figure that the GCUs and the RVU reproduce the parallel spike density modulation. We have also confirmed that the implemented FPGA can reproduce the spontaneous firing with given spontaneous firing rate and the adaptation.

TABLE I

FPGA IMPLEMENTATION. ABBREVIATIONS: FPGA = FIELD PROGRAMMABLE GATE ARRAY, GCU = GANGLION CELL UNIT, RVU = RESET VALUE UNIT, FF = FLIP FLOP, AND LUT = LOOK-UP TABLE.

Parameters of GCU and RVU	Number of GCUs	$N = 20$
	Resolutions of discrete states	$M = 273,\ L = 182$ $J = 64,\ K = 64$
Specifications of implementation	Xilinx's FPGA	XC7Z020-1CLG484C
	Number of slices	871
	Number of FFs	820
	Number of LUTs	2625
	Frequency of $C_R(t)$	100[kHz]
	Frequency of $C_i(t)$	100[kHz]
	Frequency of $C_\theta(t)$	100/15[kHz]

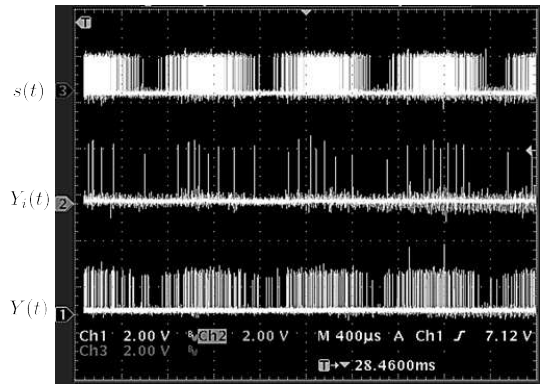

Fig. 8. FPGA experiments. Reproduction of the parallel spike density modulation. s, Y_i, Y: 2.0V/div. and time: 400μ sec/div..

V. CONCLUSIONS

As the novel spiral ganglion cell model, the RVU and the paralleled structure of the GCUs are presented, where the dynamics of the whole model is described by a special kind of asynchronous cellular automaton. It is shown that the model can reproduce some typical nonlinear responses

of the spiral ganglion cell, i.e., the spontaneous firing, the parallel spike density modulation, and the adaptation. Future problems are including the following ones: (a) more detailed analysis such as the relationship between a stimulation signal and an output spike train and (b) realizations of other nonlinear repsonses in the cochlear.

The authors would like to thank Professor Toshimitsu Ushio of Osaka Univ. for valuable discussions. This work was partially supported by the support center for advanced telecommunications technology research (SCAT) and KAKENHI Grant Number 24700225.

REFERENCES

[1] Geisler,C.D, From sound to synapse: physiology of the mammalian ear, Oxford University Press, (1997).
[2] J. O. Pickles,C.D, An introduction to the physiology of hearing, Brill Academic Pub, (2013).
[3] J. E. Rose, J. F. Brugge, D .J. Anderson and J. E. Hind, Phase-locked response to low-frequency tones in single auditory nerve fibers of the squirrel monkey, J Neurophysiol , vol. 30, pp. 769-793, (1967).
[4] L. Robles, M. A. Ruggero and N. C. Rich, Two-tone distortion in the basilar membrane of the cochlea, Nature, vol. 349, pp. 413-414 (1991).
[5] M. A. Ruggero, Responses to sound of the basilar membrane if the mammalian cochlea, Current opinion in neurobiology, vol. 2, pp. 449-456 (1992).
[6] P. G. Gillespie and J. L. Cyr, Myosin-1c, the hair cell's adaptation motor, Annu. Rev. Physiol., 66, pp. 521-545 (2004).
[7] E. G. Wever, Theory of hearing, New York : Wiley (1949).
[8] J. Wang, N. L. Powers, P. Hofstetter, P. Trautwein, D. Ding and R. Savi, Effects of selective inner hair cell loss on auditory nerve fiber threshold, tuning and spontaneous and driven discharge rate, Hearing Research, vol. 107, pp. 67-82 (1997).
[9] G. V. Békésy', Experiments in hearing, New York : McGraw-Hill (1960).
[10] H. Helmholtz, On the sensation of tone as a philosophical basis of the theory of Music, The second English edition, the fourth German edition of 1877, Dover Publications, Inc, New York, (1954).
[11] A. Kern and R. Stoop, Essential Role of Couplings between hearing nonlinearities, Physical Review Letters, vol. 91, No.12, pp. 128101. 1-128101. 4 (2003).
[12] R. Stoop and A. Kern, Two-tone suppression and combination tone generation as computations performed by Hopf cochlea, Physical Review Letters, vol. 93 (26), pp. 268103. 1-268103. 4 (2004).
[13] R. Stoop, W. -H. Steeb, J. C. Gallas and A. Kern, Auditory two-tone suppression from a subcritical Hopf cochlea, Physica A, vol. 351, pp. 175-183 (2005).
[14] V. M. Egulitz, M. Ospeck, Y. Choe, A. J. Hudspeth and M. O. Magnasco, Essential nonlinearities in hearing, Physical Review Letters, vol. 84, No. 22, pp. 5232-5235 (2000).
[15] H. Fletcher, Auditory Patterns, Reviews of modern physics, vol. 12, pp. 47-65 (1940).
[16] J. F. Schouten, Frequency analysis and periodicity detection in hearing (Plomp R, Smoorenburg GF, eds) Leiden : Sijithoff, pp. 41-58 (1970).
[17] F. A. Schaik, Analogue VLSI building Blocks for an electronic auditory pathway, EPFL, Lausanne (1997).
[18] C. Galbraith, G. M. Rebeiz, and R. Dragmeister, A cochlea-based preselector for UWB application, IEEE, Radio frequency integrated circuits symposium pp. 219-222 (2007).
[19] Louiza Sellami and Robert W. Newcomb, A digital scattering model of the cochlea, IEEE, Transactions on circuit and systems I fundamental theory and applications, vol. 44, no. 2, pp. 174-180 (1997).
[20] Vincent Chan, Shin-Chii Liu, abd André van Schaik, Aer ear: a matched silicon cochlea pair with address event representation interface, IEEE, Transaction of circuits and systems I, vol. 54, no. 1, pp. 48-59 (2007).
[21] Guan Tian, Yu Shuli, Ye Datian, Application of wavelet in speech processing of cochlear implant, IEEE, Engneering in medicine and biology 27th annual conference, Shanghai, China, pp. 5339-5342 (2005).
[22] Lloyd Watts, Reverse-engineering the human auditory pathway, WCCI, Plenary/Invited lectures, LNCS 7311, pp. 47-59 (2012).
[23] H. Torikai. and T. Nishigami, An artificial chaotic spiking neuron inspired by spiral ganglion cell: Paralleled spike encoding, theoretical analysis, and electronic circuit implementation, Neural Networks, vol. 22, Issues 5-6, pp. 664-673, (2009).
[24] T. Noguchi and H. Torikai, Ghost stochastic resonance from asynchronous cellular automaton neuron model, IEEE, Transactions on circuit and systems Ⅱ, vol. 60, No. 2, pp. 111-115 (2013).
[25] S. Hashimoto and H. Torikai, A novel hybrid spiking neuron: bifurcations, responses, and on-chip learning, IEEE, Transactions on circuit and systems, vol. 57, No. 8, pp. 2168-2181, (2010).
[26] T. Matsubara and H. Torikai, Asynchronous cellular automaton-based neuron: theoretical analysis and On-FPGA learning, IEEE, Transactions on neural networks and learning systems, vol. 24, No. 5, pp. 736-748 (2013).
[27] T. Matsubara, H. Torikai and T. Hishiki, A generalized rotate-and-fire digital spiking neuron model and its On-FPGA Learning, IEEE, Transactions on circuit and systems Ⅱ, vol. 58, No. 11, pp. 677-681 (2011).